Exciton-polariton quantum gates based on continuous variables

O. Kyriienko[1] and T. C. H. Liew[2]

[1]*The Niels Bohr Institute, University of Copenhagen, Blegdamsvej 17, DK-2100 Copenhagen, Denmark*

[2]*Division of Physics and Applied Physics, Nanyang Technological University 637371, Singapore*

(Received 29 May 2015; revised manuscript received 2 December 2015; published 4 January 2016)

We propose a continuous-variable analog of quantum controlled-NOT gates based on a system of exciton polaritons in semiconductor microcavities. This can be realized by engineering a parametric interaction between control and target polariton modes, which can be varied in time. As an explicit setup we use a system of dipolaritons, which allows for enhancement of parametric interaction by auxiliary classical fields and scalable multigate system realization. We find that high operational fidelity for the proposed gate is achievable for realistic system parameters.

DOI: 10.1103/PhysRevB.93.035301

I. INTRODUCTION

Quantum controlled-NOT (CNOT) logic gates are universal elements in quantum computation, in principle allowing the implementation of any quantum algorithm (when supplemented with single-qubit rotations). Their construction in physical systems is challenging since one requires a system with both limited dephasing and strong nonlinearity. Early realizations of CNOT gates made use of nuclear magnetic resonance in molecules [1] or postselection in linear optical systems [2], which were later reduced in size on photonic chips [3]. More recently, demonstrations of quantum gates and small quantum circuits were achieved using a variety of systems, including ion traps [4–7], nitrogen vacancy centers [8], and superconducting qubits [9–12].

Semiconductor systems have long been valued in information processing for their compact sizes, which are particularly important when one aims to build circuits with large numbers of gates. In particular, semiconductor microcavities containing quantum wells are quasi-two-dimensional structures with micron thicknesses. These structures also offer the opportunity to hybridize the properties of photons and excitons, generating new exciton-polariton quasiparticles with decay time exceeding tens of picoseconds. The presence of an excitonic component facilitates nonlinear interaction between polaritons, which has led to the experimental observation of quantum squeezing [13] as well as the theoretical [14–16] and experimental study of nonclassical correlations [17]. Additionally, macroscopically populated polaritonic modes were suggested to mimic the two-level qubit system [18] and analog CNOT gate [19]. At the same time, currently existing polaritonic samples do not possess the strong single polariton nonlinearity required for the conventional blockade mechanism [20], and most quantum effects at the weak single polariton nonlinearity level need to exploit interference effects for the realization of an unconventional polariton blockade [21–24] or generation of entangled states [25].

The aim of this paper is to introduce an alternative route toward construction of polariton quantum CNOT gates. To avoid the need for single-particle control and detection, we choose to encode information in the continuous amplitude and phase variables of polariton fields. First, a continuous-variable quantum CNOT gate operator is realized by engineering a two-mode parametric interaction Hamiltonian, which can be controlled in time. Second, it is well known that it is difficult to observe nonlinear effects when small numbers of polaritons are involved. For this reason, we exploit a mechanism of nonlinear enhancement that uses a macroscopic density to amplify scattering processes, while quantum information is maintained in separated low-density quantum modes. The proposal allows us to achieve CNOT operation fidelity as high as 99% for realistic system parameters.

Finally, we consider the scalability of our scheme, where multiple quantum gates can be cascaded one after another, in principle allowing the construction of arbitrary algorithms. Typically one imagines a quantum circuit as a network of quantum logic gates separated in space [26]. This requires that signals travel spatially between distant nodes of the network. However, spatially propagating polaritons would experience losses as they scatter with disorder and experience dispersion. While superfluidity [27–29] and bright soliton wave packets [30,31] have been shown to overcome these effects in microcavities, they imply a macroscopic classical polariton state, which cannot itself encode quantum information. In the present proposal, we use a reciprocal space encoding [32] of quantum nodes, negating the need for any spatial propagation. Polariton modes are distinguished by different momenta, and logic gates exploit momentum conservation rules to connect particular modes. Rather than being physically fixed, the gates are enacted by the application of a known pulse sequence, which could be controlled by a spatial light modulator. This brings the additional feature of being able to reconfigure the quantum circuit.

II. DEFINITIONS

The theory of quantum information with continuous variables [33] is well developed and uses the same fundamental features of quantum computation, namely superposition and entanglement, to achieve aims similar to those of qubit-based methods. Working with continuous variables, the analogous definition of the quantum CNOT gate is given by the operator $\hat{\mathrm{CN}} = e^{-i\hat{q}_1\hat{p}_2}$ [34], which acts simultaneously on two quantum fields, $\hat{a}_1$ and $\hat{a}_2$, where the amplitude and phase operators are defined by $\hat{q}_n = (\hat{a}_n + \hat{a}_n^\dagger)/\sqrt{2}$ and $\hat{p}_n = -i(\hat{a}_n - \hat{a}_n^\dagger)/\sqrt{2}$. The CNOT gate can also be defined by its action on amplitude eigenstates $\hat{\mathrm{CN}}|q_1,q_2\rangle = |q_1,q_2+q_1\rangle$, demonstrating analogy with CNOT gates: the first quantum field $\hat{a}_1$ acts as a control field, which adds to the amplitude of the target field $\hat{a}_2$.

III. SINGLE-GATE SCHEME

To realize a single CNOT gate, let us consider the Hamiltonian

$$\hat{\mathcal{H}} = \alpha(\psi^{*2}\hat{a}_1\hat{a}_2 + \psi^2\hat{a}_1^\dagger\hat{a}_2^\dagger) - J(\hat{a}_1^\dagger\hat{a}_2 + \hat{a}_2^\dagger\hat{a}_1). \quad (1)$$

It represents a parametric scattering from a macroscopically occupied mode ψ into two quantum modes $\hat{a}_1$ and $\hat{a}_2$, which have an additional linear coupling between them. If we imagine that $\hat{a}_1$ and $\hat{a}_2$ represent polariton modes with equal and opposite wave vectors, then the first term in the above Hamiltonian can be arranged making use of interbranch scattering schemes such as those studied theoretically in standard planar microcavities [35] and parametrically driven cavities [36], or experimentally in triple microcavities [37]. In such cases, the field ψ would be a polariton field with a zero in-plane wave vector, and α is a constant parametrizing the strength of polariton-polariton interactions. We will assume that ψ can be controlled optically, and ideally the linear coupling term J could also be controlled. Both resonant [38] and nonresonant [39] excitation have been used to optically generate polariton potentials, leading to the optical control of polaritons in real space [40–42], and creating the desired linear coupling J between the modes $\hat{a}_1$ and $\hat{a}_2$.

Since the amplitude and phase of ψ can be tuned, let us consider the case $\alpha\psi^2 = -J$. The phase reference of the second mode can be changed, $\hat{a}_2 \mapsto i\hat{a}_2$, following the phase of an input. Then, the Hamiltonian becomes

$$\hat{\mathcal{H}} = J(-i\hat{a}_1\hat{a}_2 + i\hat{a}_1^\dagger\hat{a}_2^\dagger - i\hat{a}_1^\dagger\hat{a}_2 + i\hat{a}_2^\dagger\hat{a}_1) = 2J\hat{q}_1\hat{p}_2, \quad (2)$$

and the corresponding evolution operator reads $\hat{\mathcal{U}} = e^{-i\hat{\mathcal{H}}t/\hbar} = e^{-i2J\hat{q}_1\hat{p}_2 t/\hbar}$. By switching the couplings on and off, the evolution time could be set to $t \to \tau_0 = \hbar/2J$, in which case the unitary evolution operator corresponds to the quantum CNOT gate. The result of CNOT gate operation can then be monitored by measuring the amplitude of a target field (see Appendix A for details of the possible detection scheme). We note that while the interaction energy between a pair of polaritons 2α may be limited, it is the quantity $\alpha\psi^2$ that determines the relevant coupling strength [43], where weak interaction is effectively amplified by the macroscopic field ψ.

IV. GATE FIDELITY

In the ideal case of unitary evolution with precisely timed parametric interaction, which we described before, the polaritonic system can work as a perfect continuous-variable CNOT gate. However, in real systems we identify the main mechanisms responsible for imperfect gate operation to be the decay of polaritons and the imprecision of the interaction constant control.

In the presence of decoherence, the evolution of any expectation value is given by

$$i\hbar\frac{d\langle\hat{A}\rangle}{dt} = \left\langle [\hat{A},\hat{\mathcal{H}}] + \frac{i\Gamma}{2}\sum_n \mathcal{L}_{\hat{a}_n}[\hat{A}] + \frac{iP}{2}\sum_n \mathcal{L}_{\hat{a}_n^\dagger}[\hat{A}] + \frac{i\Gamma_P}{2}\sum_n \mathcal{L}_{\hat{a}_n^\dagger\hat{a}_n}[\hat{A}]\right\rangle, \quad (3)$$

where Γ denotes a dissipation rate of polaritonic modes, and the Lindblad superoperator is defined as $\mathcal{L}_{\hat{a}}[\hat{A}] = 2\hat{a}^\dagger\hat{A}\hat{a} - \hat{a}^\dagger\hat{a}\hat{A} - \hat{A}\hat{a}^\dagger\hat{a}$, and Lindbladian $\mathcal{L}_{\hat{a}^\dagger\hat{a}}[\hat{A}] = 2\hat{a}^\dagger\hat{a}\hat{A}\hat{a}^\dagger\hat{a} - \hat{a}^\dagger\hat{a}\hat{a}^\dagger\hat{a}\hat{A} - \hat{A}\hat{a}^\dagger\hat{a}\hat{a}^\dagger\hat{a}$ corresponds to a pure dephasing with rate Γ_P. For the sake of generality, we also introduced an additional *incoherent* pumping at rate P with conjugate Lindbladian $\mathcal{L}_{\hat{a}^\dagger}[\hat{A}]$, which is responsible for an incoherent replenishing of polaritonic states, and it may arise from the presence of a thermal reservoir.

Using Eq. (3), we derive a closed set of evolution equations for the amplitude and phase expectation values:

$$i\hbar\frac{d\langle\hat{q}_1\rangle}{dt} = \frac{i(P-\Gamma-\Gamma_P)}{2}\langle\hat{q}_1\rangle, \quad (4)$$

$$i\hbar\frac{d\langle\hat{q}_2\rangle}{dt} = 2iJ\langle\hat{q}_1\rangle + \frac{i(P-\Gamma-\Gamma_P)}{2}\langle\hat{q}_2\rangle, \quad (5)$$

$$i\hbar\frac{d\langle\hat{p}_1\rangle}{dt} = -2iJ\langle\hat{p}_2\rangle + \frac{i(P-\Gamma-\Gamma_P)}{2}\langle\hat{p}_1\rangle, \quad (6)$$

$$i\hbar\frac{d\langle\hat{p}_2\rangle}{dt} = \frac{i(P-\Gamma-\Gamma_P)}{2}\langle\hat{p}_2\rangle, \quad (7)$$

which are readily solved analytically. One sees that for $P = \Gamma$ the mean-field amplitudes of the polaritons no longer decay, while in the regime $P > \Gamma$ one should account also for nonlinear losses [44] to prevent the amplitudes growing indefinitely. Furthermore, one can write a closed set of evolution equations for the second-order correlators ($\langle\hat{q}_1^2\rangle$, $\langle\hat{q}_1\hat{q}_2\rangle$, $\langle\hat{q}_2^2\rangle$, $\langle\hat{p}_1^2\rangle$, etc.). These equations are given in Appendix B together with their analytical solution.

To assess the performance of the quantum gate, we consider a set of displaced squeezed vacuum states as inputs, $\boldsymbol{\rho}_{\rm in} = |\psi_1\rangle\langle\psi_1| \otimes |\psi_2\rangle\langle\psi_2|$, with $|\psi_n\rangle = \hat{D}(q_n^{\rm in}, p_n^{\rm in})\hat{S}(r)|0\rangle$, where $\hat{D}(q_n^{\rm in}, p_n^{\rm in}) = \exp(\langle a_n^{\rm in}\rangle\hat{a}_n^\dagger - \langle a_n^{\rm in}\rangle^*\hat{a}_n)$ is the displacement operator providing the amplitude $q_n^{\rm in}$ and phase $p_n^{\rm in}$ of the input mean fields $\langle a_n^{\rm in}\rangle$. $\hat{S}(r) = \exp(\frac{r}{2}\hat{a}^{\dagger 2} - \frac{r}{2}\hat{a}^2)$ is the squeezing operator with squeezing parameter r, and $|0\rangle$ is the vacuum state. The ideal output state is $\boldsymbol{\rho}_{\rm ideal} = |q_1^{\rm in}, q_1^{\rm in} + q_2^{\rm in}\rangle\langle q_1^{\rm in}, q_1^{\rm in} + q_2^{\rm in}|$. The actual state $\boldsymbol{\rho}(t)$ obtained in the presence of dissipation and incoherent pumping is characterized by its fidelity with $\boldsymbol{\rho}_{\rm ideal}$:

$$F(\boldsymbol{\rho}_{\rm ideal}, \boldsymbol{\rho}(t)) = {\rm Tr}[\sqrt{\sqrt{\boldsymbol{\rho}_{\rm ideal}}\boldsymbol{\rho}(t)\sqrt{\boldsymbol{\rho}_{\rm ideal}}}]. \quad (8)$$

The fidelity can be calculated from the covariance matrix [45,46], which is directly obtained by knowing all the second-order correlators. The fidelity of the polaritonic CNOT gate as a function of decay rate is shown in Fig. 1(a) for different values of the squeezing parameter r. For each value of r, we minimize the fidelity over input states with a fixed maximum total intensity $\langle x\rangle^2 = \langle q_1\rangle^2 + \langle p_1\rangle^2 + \langle q_2\rangle^2 + \langle p_2\rangle^2$. We assume the optimum operation time $\tau_0 = \hbar/2J$. The fidelity is seen to drop from unity (corresponding to a perfect CNOT gate) monotonically as the ratio of the decay rate to the coupling strength Γ/J is increased, or when input states with a higher squeezing or total intensity are considered, as illustrated in Fig. 1(b).

The decrease of the fidelity when operating with more highly squeezed states is very natural. In phase space, the Wigner function of the unsqueezed state is a circular Gaussian, while the infinitely squeezed state is a thin line. The decay has

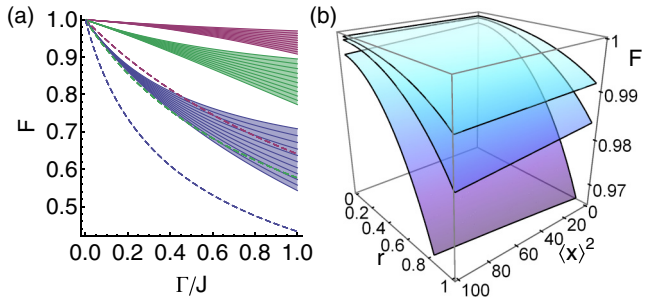

FIG. 1. (a) Fidelity of a quantum CNOT gate for increasing dissipation rate. The different colors correspond to different amounts of input squeezing (magenta: $r = 0$, green: $r = 0.5$, and blue: $r = 1$). The solid curves show the range of fidelities for total intensity increasing from $\langle x\rangle^2 = 0$ to 10, where the highest fidelity is obtained for the squeezed vacuum input. Dashed curves show the same result in the presence of an additional incoherent pumping, chosen with rate $P = \Gamma$. (b) Dependence of the minimum fidelity of the input squeezing r and total intensity $\langle x\rangle^2$. The different surfaces correspond to different values of $\Gamma/J = (0.01, 0.02, 0.05)$. Smaller values of Γ/J leading to very high fidelities are expected in samples with a high quality factor.

the effect of smearing any squeezed state into the unsqueezed state with $\langle q_n^2\rangle = \langle p_n^2\rangle = 1/2$. In fact, the state is driven toward the unsqueezed state at a rate proportional to $1/2 - \langle q^2\rangle$ (as can be seen from writing the correlator evolution explicitly), that is, highly squeezed states are most quickly deformed in phase space.

The dashed curves show the fidelities calculated with a nonzero incoherent pump, which attempts to compensate the losses in the system ($P = \Gamma$). Interestingly, in this case the fidelity no longer depends on the intensity of the initial state, however it becomes worse due to the incoherent pump. While the incoherent pump can compensate fully for the loss of mean-field amplitudes, it cannot compensate for the loss of quantum correlations caused by dissipation. Allowing for different values of P, one finds that the optimum fidelity appears for $P = 0$.

Next, we plot the dependence of gate fidelity on the pure dephasing rate. The results are shown in Fig. 2(a) assuming

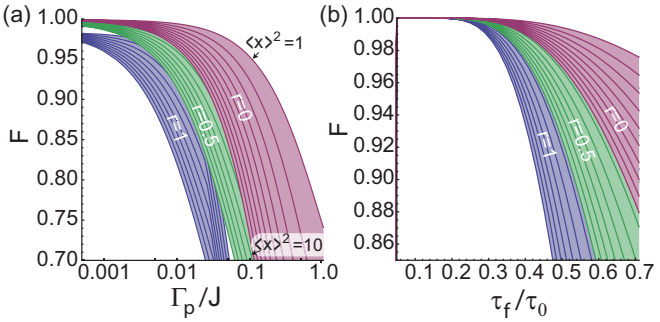

FIG. 2. Range of CNOT fidelities calculated for input states of total intensity increasing from $\langle x\rangle^2 = 1$ to 10, accounting for a pure dephasing and nonideal gate pulse. (a) Fidelity as a function of pure dephasing rate for input states with squeezing parameter $r = 0, 0.5, 1$. (b) Gate fidelity in square $J(t)$ pulse operation mode plotted as a function of signal edge time to optimal operation time ratio, τ_f/t_0.

the decay rate $\Gamma/J = 0.02$, input states with $r = 0, 0.5, 1$, and varying total intensity ranging from $\langle x\rangle^2 = 1$ to 10. These suggest that a low level of pure dephasing $\Gamma_P/J < 0.05$ is required for high-quality CNOT operation.

Additionally, we study the influence of imperfect timing of the gate pulse on the fidelity of the continuous variable CNOT gate. We start by considering a square pulse with finite pulse edges described by $J(t) = J_0 f(t)[1 - f(t - \tau_0)]$, where $f(t) = [\exp(-t/\tau_f) + 1]^{-1}$, with τ_f being the pulse edge time, and J_0 denotes a time-independent interaction constant. The fidelity as a function of pulse edge time is shown in Fig. 2(b) for an ideal case of negligible losses. The results suggest that an accurate control of the gate pulse is required at a time scale below $\hbar/J_0$, where pulses with sharp edges, $\tau_f/\tau_0 < 0.3$, do not contribute to degradation of the gate fidelity.

Finally, we discuss the experimental feasibility of the proposed scheme, with the main parameters being the polariton lifetime, the nonlinear coupling constant, pure dephasing, and the characteristic switching time. Polariton lifetimes $\tau_{\rm dec}$ in the range of hundreds of picoseconds have been reported recently [47,48], with the corresponding decay rate being in the μeV range. When controlled with a classical field, nonlinearities can be tuned to be in the sub-meV range. Taking $J = 0.2$ meV and $\tau_{\rm dec} = 65$ ps gives the ratio of $\Gamma/J \approx 0.02$, and it sets the characteristic switching time to a picosecond range, which will be achievable with an optical control of the coupling constant. The pure dephasing in the polaritonic system was estimated to be at the $\Gamma_P = 0.2$ μeV level [49], yielding $\Gamma_P/J = 10^{-3}$. This makes high fidelities of 99% feasible for input states of $\langle x^2\rangle < 10$ and $r \approx 0.5$.

V. MULTIGATE SYSTEM: DIPOLARITON SETUP

We now discuss a scalable scheme of CNOT gates, which requires a set of multiple quantum modes and the ability to apply successive gates between chosen pairs of modes. Toward that end, let us consider a dipolariton system [50], in which two types of exciton modes (direct and indirect) are coupled to a cavity mode in a microcavity, resulting in three dispersion branches as illustrated in Fig. 3. The advantage of the dipolariton system is the freedom in varying the mode energies via an applied electric field, although similar setups could be imagined in triple microcavities [37].

Each dispersion mode exhibits a linear polarization splitting between the transverse-electric (TE) and transverse-magnetic (TM) polarizations [51]. Let us take the TM-polarized modes of the middle branch as the relevant quantum modes of our system. A degenerate set of these modes can be distinguished by different orientations of in-plane wave vector, and they are illustrated in green in Fig. 3. In the following, we will choose to work in the frame rotating at the energy of this set of modes.

The Hamiltonian of the multimode system up to an energy shift reads (see details in Appendix C)

$$\begin{aligned}\hat{\mathcal{H}} =& A\psi_{\mathrm{UP},+}\psi_{\mathrm{LP},+}\hat{a}^\dagger_{2,+}\hat{a}^\dagger_{1,+} + B\psi'^*_{\mathrm{LP},-}\psi_{\mathrm{LP},-}\hat{a}^\dagger_{2,-}\hat{a}_{1,-}\\ &+ C\psi_{\mathrm{UP},+}\psi_{\mathrm{LP},-}\hat{a}^\dagger_{2,+}\hat{a}^\dagger_{1,-}\\ &+ D\psi'^*_{\mathrm{LP},-}\psi_{\mathrm{LP},-}\hat{a}^\dagger_{2,+}\hat{a}_{1,+} + \mathrm{H.c.},\end{aligned} \tag{9}$$

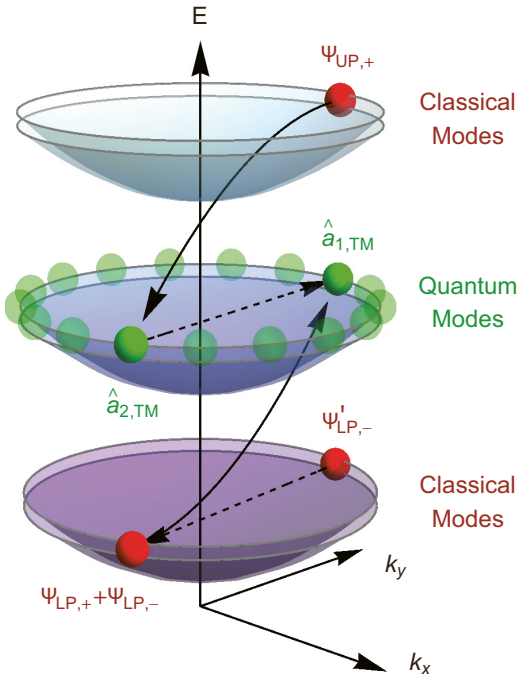

FIG. 3. Scheme for a CNOT gate implemented between a selected pair of modes. The plot shows 2D dispersion of three polaritonic modes, each split in two branches for different polarization components.

where A, B, C, and D are effective interaction constants that depend on Hopfield coefficients and bare interactions. Here $\psi_{\alpha,j}$ denote the relevant classical modes.

The quantum modes can be rewritten in terms of their TE- and TM-polarized components using the transformation

$$(\hat{a}_{n,+}\hat{a}_{n,-}) = \frac{1}{\sqrt{2}}\begin{pmatrix} e^{2i\phi_n} & ie^{2i\phi_n} \\ e^{-2i\phi_n} & -ie^{-2i\phi_n} \end{pmatrix}(\hat{a}_{n,\mathrm{TM}}\hat{a}_{n,\mathrm{TE}}), \quad (10)$$

where ϕ_n denotes the angle of the mode n in reciprocal space.

To arrange for a CNOT gate between an arbitrary pair of modes, $\hat{a}_{1,\mathrm{TM}}$ and $\hat{a}_{2,\mathrm{TM}}$, we consider a quite specific but fully feasible macroscopic excitation of classical fields in the lower and upper polariton branches, as illustrated in red in Fig. 3. In the upper branch, we choose a circularly polarized field $\psi_{\mathrm{UP},+}$ at the same wave vector as $\hat{a}_{1,\mathrm{TM}}$. In the lower branch, we choose a cross-circularly-polarized field $\psi'_{\mathrm{LP},-}$ for instance to have the same wave vector as $\hat{a}_{1,\mathrm{TM}}$, together with a linear polarization (characterized by a superposition of both circular components $\psi_{\mathrm{LP},+}$ and $\psi_{\mathrm{LP},-}$) at the same wave vector as $\hat{a}_{2,\mathrm{TM}}$. Since we have chosen classical fields with the same in-plane wave vectors as $\hat{a}_{1,\mathrm{TM}}$ or $\hat{a}_{2,\mathrm{TM}}$, momentum conservation rules allow only a coupling of the chosen quantum modes by the classical fields. In particular, two types of scattering processes appear, where interactions between parallel spins are considered. First, the σ_+-polarized component of the pumping provides an effective two-mode squeezing interaction, allowing for the scattering processes indicated by the solid arrows in Fig. 3 (the reverse scattering process also occurs). Second, the σ_--polarized component of the pumping results in a process in which the quantum modes are exchanged by transferring their momentum to the classical field. This process is indicated by the dashed arrows in Fig. 3 (and again the reverse process also occurs). Finally, the classical field energies can be chosen such that the relevant scattering processes are resonant only with the TM-polarized states. Neglecting off-resonant interactions with TE states (see the discussion in Appendix D) gives the Hamiltonian

$$\hat{\mathcal{H}} = iJ\hat{a}^\dagger_{1,\mathrm{TM}}\hat{a}^\dagger_{2,\mathrm{TM}} + iJ\hat{a}^\dagger_{2,\mathrm{TM}}\hat{a}_{1,\mathrm{TM}} + \mathrm{H.c.}, \quad (11)$$

where J can be made real by correct choice of the amplitudes and phases of the classical fields (Appendix C), allowing for CNOT operations acting on eight different continuous variable modes.

VI. CONCLUSION

We presented a scheme for quantum logic gates based on exciton polaritons in semiconductor microcavities. Unlike previous schemes, we operate with continuous variables that avoid the necessity of operating with a definite number of polaritons, and we make use of an effective amplification of nonlinearity in the system based on the coupling of quantum modes with macroscopically occupied classical states. Using these ingredients, a quantum optical treatment of decay processes predicts fidelities in excess of 99% for existing microcavities. Additionally, we proposed a way to construct scalable networks of polaritonic gates. The experimental demonstration of our proposal would not be reliant on single-photon detection and would require standard homodyne detection measurements (this would depend also on the implementation of future error-correction protocols).

APPENDIX A: POSSIBLE IMPLEMENTATION OF AN EXPERIMENTAL DETECTION SCHEME

The characterization of a quantum optical process can be achieved by measuring its effect on input coherent states [52]. Gaussian coherent states are fully characterized by their covariance matrix, which can be experimentally accessed using homodyne detection [53]. An important ingredient of such a technique is the availability of a classical local oscillator, with frequency identical to that of the measured modes. While this is not immediately available in our system, a modified detection scheme can be implemented using an additional interference between the lasers driving upper- and lower-branch polaritons.

For the described system, the relevant two-mode covariance matrix is given by

$$V_{ij} = \tfrac{1}{2}\langle \hat{x}_i\hat{x}_j + \hat{x}_j\hat{x}_i\rangle - \langle \hat{x}_i\rangle\langle \hat{x}_j\rangle, \quad (A1)$$

where $\hat{x}^T = (\hat{q}_1, \hat{p}_1, \hat{q}_2, \hat{p}_2)$.

From the interference of the modes $\hat{a}_1$ and $\hat{a}_2$ on a beamsplitter and the application of phase delays, one has access to the fields $\hat{a}_3 = (\hat{a}_1 + \hat{a}_2)/\sqrt{2}$, $\hat{a}_4 = (\hat{a}_1 - \hat{a}_2)/\sqrt{2}$, $\hat{a}_5 = (i\hat{a}_1 + \hat{a}_2)/\sqrt{2}$, and $\hat{a}_6 = (i\hat{a}_1 - \hat{a}_2)/\sqrt{2}$ [see Fig. 4(a)].

The fields $\hat{a}_i$ all oscillate at the same frequency, which is midway between the frequency of the laser driving the upper polariton branch and the frequency of the laser driving the lower polariton branch. Let us consider interfering any of the fields $\hat{a}_i$ on a beamsplitter with a local oscillator field of the form $\alpha_{\mathrm{LO}}(e^{i\Omega t} + e^{-i\Omega t})$. This form of local oscillator

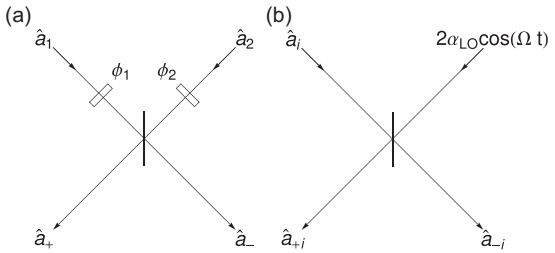

FIG. 4. Experimental scheme for measurement of a covariance matrix. (a) Using phase delays (ϕ_1, ϕ_2) and interfering on a beamsplitter generates the fields $\hat{a}_\pm = (\hat{a}_1 e^{i\phi_1} \pm \hat{a}_2 e^{i\phi_2})/\sqrt{2}$. Different combinations of phases then allow access to the fields $\hat{a}_i$ as defined in the text. (b) Interfering $\hat{a}_i$ with a local oscillator of the form $\alpha_{LO}(e^{i\Omega t} + e^{-i\Omega t})$ allows for the generation of the fields $\hat{a}_{\pm i} = [\hat{a}_i \pm \alpha_{LO}(e^{i\Omega t} + e^{-i\Omega t})]/\sqrt{2}$. The differences of the corresponding photocurrents give access to the quadratures of $\hat{a}_i$.

can be attained from the superposition of the lasers driving the lower and upper branches, where α_{LO} is the (complex) field amplitude and Ω is the frequency difference with the middle polariton modes. The photocurrents obtained at each of the output ports are [see Fig. 4(b)]

$$\hat{n}_{+i} = \tfrac{1}{2}(\hat{a}_i^\dagger + \alpha_{LO}^*(e^{i\Omega t} + e^{-i\Omega t}))[\hat{a}_i + \alpha_{LO}(e^{i\Omega t} + e^{-i\Omega t})], \tag{A2}$$

$$\hat{n}_{-i} = \tfrac{1}{2}(\hat{a}_i^\dagger - \alpha_{LO}^*(e^{i\Omega t} + e^{-i\Omega t}))[\hat{a}_i - \alpha_{LO}(e^{i\Omega t} + e^{-i\Omega t})]. \tag{A3}$$

The difference photocurrent is then

$$\hat{n}_{+i} - \hat{n}_{-i} = 2(\hat{a}_i^\dagger \alpha_{LO} + \hat{a}_i \alpha_{LO}^*)\cos(\Omega t). \tag{A4}$$

The $\cos(\Omega t)$ modulation can be identified and demodulated. By varying the phase of α_{LO}, one can access $\langle \hat{a}_i^\dagger \pm \hat{a}_i \rangle$ from the average values and $\langle (\hat{a}_i^\dagger \pm \hat{a}_i)^2 \rangle$ from the observed variation. From these quantities, the covariance matrix can be reconstructed as in Ref. [53].

APPENDIX B: ANALYTIC SOLUTION OF THE FIRST- AND SECOND-ORDER CORRELATOR EVOLUTION

To calculate the fidelity of the polaritonic CNOT gate as a function of decay rate Γ and pure dephasing rate Γ_P, we derive the analytic solutions for amplitude and phase expectation values, as wells as higher-order correlators. The solution of Eqs. (4)–(7) in the main text reads

$$\langle \hat{q}_1(t) \rangle = \langle \hat{q}_1(0) \rangle e^{(P-\Gamma-\Gamma_P)t/(2\hbar)}, \tag{B1}$$

$$\langle \hat{q}_2(t) \rangle = e^{(P-\Gamma-\Gamma_P)t/(2\hbar)} \left(\langle \hat{q}_2(0) \rangle + \frac{2J}{\hbar} \langle \hat{q}_1(0) \rangle t \right), \tag{B2}$$

$$\langle \hat{p}_1(t) \rangle = e^{(P-\Gamma-\Gamma_P)t/(2\hbar)} \left(\langle \hat{p}_1(0) \rangle - \frac{2J}{\hbar} \langle \hat{p}_2(0) \rangle t \right), \tag{B3}$$

$$\langle \hat{p}_2(t) \rangle = \langle \hat{p}_2(0) \rangle e^{(P-\Gamma-\Gamma_P)t/(2\hbar)}, \tag{B4}$$

where $\langle \hat{q}_n(0) \rangle$ and $\langle \hat{p}_n(0) \rangle$ represent the initial amplitude and phase mean-field values.

The evolution of second-order correlators can be derived from Eq. (3) as

$$i\hbar \frac{d\langle \hat{q}_1^2 \rangle}{dt} = \frac{i\Gamma}{2}\left(1 - 2\langle \hat{q}_1^2 \rangle\right) + \frac{iP}{2}\left(1 + 2\langle \hat{q}_1^2 \rangle\right) - i\Gamma_P\left(\langle \hat{q}_1^2 \rangle - \langle \hat{p}_1^2 \rangle\right), \tag{B5}$$

$$i\hbar \frac{d\langle \hat{q}_1 \hat{q}_2 \rangle}{dt} = 2iJ\langle \hat{q}_1^2 \rangle + i(P - \Gamma - 2\Gamma_P)\langle \hat{q}_1 \hat{q}_2 \rangle, \tag{B6}$$

$$i\hbar \frac{d\langle \hat{q}_2^2 \rangle}{dt} = 4iJ\langle \hat{q}_1 \hat{q}_2 \rangle + \frac{i\Gamma}{2}\left(1 - 2\langle \hat{q}_2^2 \rangle\right) + \frac{iP}{2}\left(1 + 2\langle \hat{q}_2^2 \rangle\right) - i\Gamma_P\left(\langle \hat{q}_2^2 \rangle - \langle \hat{p}_2^2 \rangle\right), \tag{B7}$$

$$i\hbar \frac{d\langle \hat{p}_1^2 \rangle}{dt} = -4iJ\langle \hat{p}_1 \hat{p}_2 \rangle + \frac{i\Gamma}{2}\left(1 - 2\langle \hat{p}_1^2 \rangle\right) + \frac{iP}{2}\left(1 + 2\langle \hat{p}_1^2 \rangle\right) - i\Gamma_P\left(\langle \hat{p}_1^2 \rangle - \langle \hat{q}_1^2 \rangle\right), \tag{B8}$$

$$i\hbar \frac{d\langle \hat{p}_1 \hat{p}_2 \rangle}{dt} = -2iJ\langle \hat{p}_2^2 \rangle + i(P - \Gamma - 2\Gamma_P)\langle \hat{p}_1 \hat{p}_2 \rangle, \tag{B9}$$

$$i\hbar \frac{d\langle \hat{p}_2^2 \rangle}{dt} = \frac{i\Gamma}{2}\left(1 - 2\langle \hat{p}_2^2 \rangle\right) + \frac{iP}{2}\left(1 + 2\langle \hat{p}_2^2 \rangle\right) - i\Gamma_P\left(\langle \hat{p}_2^2 \rangle - \langle \hat{q}_2^2 \rangle\right), \tag{B10}$$

$$i\hbar \frac{\langle \hat{q}_1 \hat{p}_2 \rangle}{dt} = i(P - \Gamma - 2\Gamma_P)\langle \hat{q}_1 \hat{p}_2 \rangle, \tag{B11}$$

$$i\hbar \frac{\langle \hat{q}_1 \hat{p}_1 \rangle}{dt} = -2iJ\langle \hat{q}_1 \hat{p}_2 \rangle + \tfrac{i(P-\Gamma-2\Gamma_P)}{2}(2\langle \hat{q}_1 \hat{p}_1 \rangle - i), \tag{B12}$$

$$i\hbar \frac{\langle \hat{q}_2 \hat{p}_1 \rangle}{dt} = 2iJ(\langle \hat{q}_1 \hat{p}_1 \rangle - \langle \hat{q}_2 \hat{p}_2 \rangle) + i(P - \Gamma - 2\Gamma_P)\langle \hat{q}_2 \hat{p}_1 \rangle, \tag{B13}$$

$$i\hbar \frac{\langle \hat{q}_2 \hat{p}_2 \rangle}{dt} = 2iJ\langle \hat{q}_1 \hat{p}_2 \rangle + \tfrac{i(P-\Gamma-2\Gamma_P)}{2}(2\langle \hat{q}_2 \hat{p}_2 \rangle - i). \tag{B14}$$

Equations (B5)–(B14) can be solved analytically for $\Gamma_P = 0$ and $\Gamma \neq P$, giving

$$\langle \hat{q}_1^2(t) \rangle = c_1 + \left[\langle \hat{q}_1^2(0) \rangle - c_1\right] e^{(P-\Gamma)t/\hbar}, \tag{B15}$$

$$\langle \hat{q}_1(t)\hat{q}_2(t) \rangle = c_2 + [\langle \hat{q}_1(0)\hat{q}_2(0) \rangle - c_2] e^{(P-\Gamma)t/\hbar} + \left(c_3 + \frac{2J}{\hbar}\langle \hat{q}_1^2(0) \rangle\right) t e^{(P-\Gamma)t/\hbar}, \tag{B16}$$

$$\langle \hat{q}_2^2(t) \rangle = c_4 + \left(\langle \hat{q}_2^2(0) \rangle - c_4 + \frac{4J[\langle \hat{q}_1 \hat{q}_2(0) \rangle - c_2]}{\hbar} t + \frac{2J\left[c_3\hbar + 2J\langle \hat{q}_1^2(0) \rangle\right]}{\hbar^2} t^2\right) e^{(P-\Gamma)t/\hbar}, \tag{B17}$$

$$\langle \hat{p}_2^2(t) \rangle = c_1 + \left[\langle \hat{p}_2^2(0) \rangle - c_1\right] e^{(P-\Gamma)t/\hbar}, \tag{B18}$$

$$\langle \hat{p}_1(t)\hat{p}_2(t) \rangle = -c_2 + [\langle \hat{p}_1(0)\hat{p}_2(0) \rangle + c_2] e^{(P-\Gamma)t/\hbar} - \left(c_3 + \frac{2J}{\hbar}\langle \hat{p}_2^2(0) \rangle\right) t e^{(P-\Gamma)t/\hbar}, \tag{B19}$$

$$\langle \hat{p}_1^2(t)\rangle = c_4 + \left(\langle \hat{p}_1^2(0)\rangle - c_4 - \frac{4J[\langle \hat{p}_1\hat{p}_2(0)\rangle + c_2]}{\hbar}t + \frac{2J\left[c_3\hbar + 2J\langle \hat{p}_2^2(0)\rangle\right]}{\hbar^2}t^2\right)e^{(P-\Gamma)t/\hbar}, \quad \text{(B20)}$$

$$\langle \hat{q}_1\hat{p}_2(t)\rangle = \langle \hat{q}_1\hat{p}_2(0)\rangle e^{(P-\Gamma)t/\hbar}, \quad \text{(B21)}$$

$$\langle \hat{q}_1\hat{p}_1(t)\rangle = \frac{i}{2} + \left(\langle \hat{q}_1\hat{p}_1(0)\rangle - \frac{i}{2} - \frac{2J\langle \hat{q}_1\hat{p}_2(0)\rangle t}{\hbar}\right)e^{(P-\Gamma)t/\hbar}, \quad \text{(B22)}$$

$$\langle \hat{q}_2\hat{p}_2(t)\rangle = \frac{i}{2} + \left(\langle \hat{q}_2\hat{p}_2(0)\rangle - \frac{i}{2} + \frac{2J\langle \hat{q}_1\hat{p}_2(0)\rangle t}{\hbar}\right)e^{(P-\Gamma)t/\hbar}, \quad \text{(B23)}$$

$$\langle \hat{q}_2\hat{p}_1(t)\rangle = \left(\langle \hat{q}_2\hat{p}_1(0)\rangle + \frac{2J}{\hbar}[\langle \hat{q}_1\hat{p}_1(0)\rangle - \langle \hat{q}_2\hat{p}_2(0)\rangle]t - \frac{4J^2\langle \hat{q}_1\hat{p}_2(0)\rangle t^2}{\hbar^2}\right)e^{(P-\Gamma)t/\hbar}, \quad \text{(B24)}$$

where the coefficients are

$$c_1 = \frac{P+\Gamma}{2(\Gamma - P)}, \quad \text{(B25)}$$

$$c_2 = \frac{2c_1 J}{\Gamma - P}, \quad \text{(B26)}$$

$$c_3 = -2c_1\frac{J}{\hbar}, \quad \text{(B27)}$$

$$c_4 = c_1 + \frac{4c_2 J}{\Gamma - P}. \quad \text{(B28)}$$

Separate equations hold for the special case $\Gamma = P$.

APPENDIX C: MULTIGATE REALIZATION: DETAILED DESCRIPTION

In the main text of the paper, we described the scheme for a multi-CNOT gate, which can operate on different pairs of continuous-variable modes, encoded by the planar wave vector. The following can be done, for instance, in the spinor dipolaritonic system, where direct exciton (DX), indirect exciton (IX), and cavity photon (C) form three distinct dipolaritonic modes UP, MP, and LP, with associated parametric scattering between them. Alternatively, one can envisage a similar system, where two different direct exciton modes DX_1 and DX_2 are coupled to the same cavity mode C.

We start the description from a generic dipolaritonic Hamiltonian [43,54]

$$\hat{\mathcal{H}}_{\rm dip} = \hat{\mathcal{H}}_0 + \hat{\mathcal{H}}_{\rm int}, \quad \text{(C1)}$$

where we separated the linear Hamiltonian of bare modes and associated couplings, $\hat{\mathcal{H}}_0$, and the interaction Hamiltonian $\hat{\mathcal{H}}_{\rm int}$ coming from exciton-exciton interactions.

The linear part reads

$$\hat{\mathcal{H}}_0 = \sum_{\mathbf{k},j=\pm} E_{{\rm C},\mathbf{k},j}\hat{a}^\dagger_{\mathbf{k},j}\hat{a}_{\mathbf{k},j} + \sum_{\mathbf{k},j=\pm} E_{{\rm DX},\mathbf{k},j}\hat{b}^\dagger_{\mathbf{k},j}\hat{b}_{\mathbf{k},j} + \sum_{\mathbf{k},j=\pm} E_{{\rm IX},\mathbf{k},j}\hat{c}^\dagger_{\mathbf{k},j}\hat{c}_{\mathbf{k},j} + \sum_{\mathbf{k},j=\pm} \Omega_{\text{C-DX}}(\hat{a}^\dagger_{\mathbf{k},j}\hat{b}_{\mathbf{k},j} + \hat{b}^\dagger_{\mathbf{k},j}\hat{a}_{\mathbf{k},j}) - \sum_{\mathbf{k},j=\pm} J_{\text{DX-IX}}(\hat{a}^\dagger_{\mathbf{k},j}\hat{b}_{\mathbf{k},j} + \hat{b}^\dagger_{\mathbf{k},j}\hat{a}_{\mathbf{k},j}), \quad \text{(C2)}$$

where $\hat{a}_{\mathbf{k},j}$ ($\hat{a}^\dagger_{\mathbf{k},j}$), $\hat{b}_{\mathbf{k},j}$ ($\hat{b}^\dagger_{\mathbf{k},j}$), and $\hat{c}_{\mathbf{k},j}$ ($\hat{c}^\dagger_{\mathbf{k},j}$) correspond to annihilation (creation) operators of the cavity photon, direct exciton, and indirect exciton modes with $\mathbf{k}$ planar wave vector and $j = \pm$ circular polarization, respectively. The dispersions of the C, DX, and IX modes are $E_{{\rm C},\mathbf{k},j}$, $E_{{\rm DX},\mathbf{k},j}$, and $E_{{\rm IX},\mathbf{k},j}$, respectively, and we consider circular modes to be degenerate in energy, $E_{\cdot,\mathbf{k},+} = E_{\cdot,\mathbf{k},-}$. $\Omega_{\text{C-DX}}$ corresponds to the exciton-photon coupling constant, and $J_{\text{DX-IX}}$ denotes tunneling coupling between adjacent quantum wells.

The interaction Hamiltonian can be written as

$$\hat{\mathcal{H}}_{\rm int} = \hat{\mathcal{H}}_{\text{DX-DX}} + \hat{\mathcal{H}}_{\text{IX-IX}} + \hat{\mathcal{H}}_{\text{DX-IX}}, \quad \text{(C3)}$$

where we separate contributions emerging from direct exciton interaction, indirect exciton interaction, and direct-indirect cross-Kerr interaction. Starting from conventional DX-DX interaction, the Hamiltonian reads

$$\begin{aligned}\hat{\mathcal{H}}_{\text{DX-DX}} = &\sum_{\mathbf{k},\mathbf{k}',\mathbf{q}} \alpha_1^{\rm DD}(\mathbf{k},\mathbf{k}',\mathbf{q})\hat{b}^\dagger_{\mathbf{k}-\mathbf{q},+}\hat{b}^\dagger_{\mathbf{k}'+\mathbf{q},+}\hat{b}_{\mathbf{k},+}\hat{b}_{\mathbf{k}',+} \\ &+ \sum_{\mathbf{k},\mathbf{k}',\mathbf{q}} \alpha_1^{\rm DD}(\mathbf{k},\mathbf{k}',\mathbf{q})\hat{b}^\dagger_{\mathbf{k}-\mathbf{q},-}\hat{b}^\dagger_{\mathbf{k}'+\mathbf{q},-}\hat{b}_{\mathbf{k},-}\hat{b}_{\mathbf{k}',-} \\ &+ \sum_{\mathbf{k},\mathbf{k}',\mathbf{q}} \alpha_2^{\rm DD}(\mathbf{k},\mathbf{k}',\mathbf{q})\hat{b}^\dagger_{\mathbf{k}-\mathbf{q},+}\hat{b}_{\mathbf{k},+}\hat{b}^\dagger_{\mathbf{k}'+\mathbf{q},-}\hat{b}_{\mathbf{k}',-} \\ &+ \sum_{\mathbf{k},\mathbf{k}',\mathbf{q}} \alpha_2^{\rm DD}(\mathbf{k},\mathbf{k}',\mathbf{q})\hat{b}^\dagger_{\mathbf{k}-\mathbf{q},-}\hat{b}_{\mathbf{k},-}\hat{b}^\dagger_{\mathbf{k}'+\mathbf{q},+}\hat{b}_{\mathbf{k}',+},\end{aligned} \quad \text{(C4)}$$

where $\alpha_1^{\rm DD}$ corresponds to the triplet or cocircular Coulomb interaction between direct excitons of the same spin, and $\alpha_2^{\rm DD}$ is the singlet or cross-circular interaction between direct excitons of opposite polarization. We note that for relevant momenta of the polaritonic system, the exciton-exciton interaction constant is momentum-independent and can be typically treated as a constant.

In the following, we are interested in particular wave vectors of the particles, namely the one where scattering happens between initial states of $\mathbf{k}_2$ and $\mathbf{k}_1$ and final states $\mathbf{k}_1'$ and $\mathbf{k}_2'$ chosen according to momentum conservation. Using this labeling, Eq. (C4) yields

$$\begin{aligned}\hat{\mathcal{H}}_{\text{DX-DX}} = &\alpha_1^{\rm DD}\hat{b}^\dagger_{\mathbf{k}_2',+}\hat{b}^\dagger_{\mathbf{k}_1',+}\hat{b}_{\mathbf{k}_2,+}\hat{b}_{\mathbf{k}_1,+} + \alpha_1^{\rm DD}\hat{b}^\dagger_{\mathbf{k}_2',-}\hat{b}^\dagger_{\mathbf{k}_1',-}\hat{b}_{\mathbf{k}_2,-}\hat{b}_{\mathbf{k}_1,-} \\ &+ \alpha_2^{\rm DD}\hat{b}^\dagger_{\mathbf{k}_2',+}\hat{b}_{\mathbf{k}_2,+}\hat{b}^\dagger_{\mathbf{k}_1',-}\hat{b}_{\mathbf{k}_1,-} \\ &+ \alpha_2^{\rm DD}\hat{b}^\dagger_{\mathbf{k}_2',-}\hat{b}_{\mathbf{k}_2,-}\hat{b}^\dagger_{\mathbf{k}_1',+}\hat{b}_{\mathbf{k}_1,+}.\end{aligned} \quad \text{(C5)}$$

The interaction terms for indirect excitons can be written in a similar fashion, giving

$$\begin{aligned}\hat{\mathcal{H}}_{\text{IX-IX}} = &\alpha_1^{\rm II}\hat{c}^\dagger_{\mathbf{k}_2',+}\hat{c}^\dagger_{\mathbf{k}_1',+}\hat{c}_{\mathbf{k}_2,+}\hat{c}_{\mathbf{k}_1,+} + \alpha_1^{\rm II}\hat{c}^\dagger_{\mathbf{k}_2',-}\hat{c}^\dagger_{\mathbf{k}_1',-}\hat{c}_{\mathbf{k}_2,-}\hat{c}_{\mathbf{k}_1,-} \\ &+ \alpha_2^{\rm II}\hat{c}^\dagger_{\mathbf{k}_2',+}\hat{c}_{\mathbf{k}_2,+}\hat{c}^\dagger_{\mathbf{k}_1',-}\hat{c}_{\mathbf{k}_1,-} \\ &+ \alpha_2^{\rm II}\hat{c}^\dagger_{\mathbf{k}_2',-}\hat{c}_{\mathbf{k}_2,-}\hat{c}^\dagger_{\mathbf{k}_1',+}\hat{c}_{\mathbf{k}_1,+},\end{aligned} \quad \text{(C6)}$$

with $\alpha^{\mathrm{II}}_{1,2}$ triplet/singlet interaction between spinor indirect excitons. The cross-interaction between direct and indirect excitons reads

$$\hat{\mathcal{H}}_{\text{DX-IX}} = \alpha^{\mathrm{DI}}_1 \hat{b}^\dagger_{\mathbf{k}'_2,+}\hat{c}^\dagger_{\mathbf{k}'_1,+}\hat{b}_{\mathbf{k}_2,+}\hat{c}_{\mathbf{k}_1,+} + \alpha^{\mathrm{DI}}_1 \hat{b}^\dagger_{\mathbf{k}'_2,-}\hat{c}^\dagger_{\mathbf{k}'_1,-}\hat{b}_{\mathbf{k}_2,-}\hat{c}_{\mathbf{k}_1,-} + \alpha^{\mathrm{DI}}_2 \hat{b}^\dagger_{\mathbf{k}'_2,+}\hat{b}_{\mathbf{k}_2,+}\hat{c}^\dagger_{\mathbf{k}'_1,-}\hat{c}_{\mathbf{k}_1,-} + \alpha^{\mathrm{DI}}_2 \hat{b}^\dagger_{\mathbf{k}'_2,-}\hat{b}_{\mathbf{k}_2,-}\hat{c}^\dagger_{\mathbf{k}'_1,+}\hat{c}_{\mathbf{k}_1,+}, \tag{C7}$$

where $\alpha^{\mathrm{DI}}_{1,2}$ corresponds to direct-indirect exciton Coulomb interaction for the same and opposite spin projections ± 1.

Next, we perform the transformation of the linear Hamiltonian (C2) to the diagonal basis of dipolariton operators $\hat{A}_j$ ($j = 1,2,3$):

$$\hat{a}_{k,\pm} = V_{11,k,\pm}\hat{A}_{1,k,\pm} + V_{21,k,\pm}\hat{A}_{2,k,\pm} + V_{31,k,\pm}\hat{A}_{3,k,\pm}, \tag{C8}$$

$$\hat{b}_{k,\pm} = V_{12,k,\pm}\hat{A}_{1,k,\pm} + V_{22,k,\pm}\hat{A}_{2,k,\pm} + V_{32,k,\pm}\hat{A}_{3,k,\pm}, \tag{C9}$$

$$\hat{c}_{k,\pm} = V_{13,k,\pm}\hat{A}_{1,k,\pm} + V_{23,k,\pm}\hat{A}_{2,k,\pm} + V_{33,k,\pm}\hat{A}_{3,k,\pm}, \tag{C10}$$

where V_{ij} are the matrix elements of eigenvectors, corresponding to dipolariton Hopfield coefficients. Without limiting the generality, we consider V_{ij} to be real for any i and j.

The transformed linear part reads

$$\hat{\mathcal{H}}'_0 = \sum_{j,\mathbf{k},\pm} E_{j,\mathbf{k},\pm}\hat{A}^\dagger_{j,\mathbf{k},\pm}\hat{A}_{j,\mathbf{k},\pm}. \tag{C11}$$

The eigenenergies possess rotation symmetry, $E_j(\mathbf{k}) = E_j(k)$, and thus the Hopfield coefficients are spin-independent, $V_{ij,\mathbf{k},\pm} \equiv V_{ij}$, where we omit the momentum index for brevity.

We proceed with the transformation of the interaction Hamiltonian by successive transformation of its parts. For instance, the direct exciton interaction part can be rewritten as

$$\begin{aligned}
\hat{\mathcal{H}}'_{\text{DX-DX}} = {} & \alpha^{\mathrm{DD}}_1\big(V_{12}\hat{A}^\dagger_{1,\mathbf{k}'_2,+} + V_{22}\hat{A}^\dagger_{2,\mathbf{k}'_2,+} + V_{32}\hat{A}^\dagger_{3,\mathbf{k}'_2,+}\big)\big(V_{12}\hat{A}^\dagger_{1,\mathbf{k}'_1,+} + V_{22}\hat{A}^\dagger_{2,\mathbf{k}'_1,+} + V_{32}\hat{A}^\dagger_{3,\mathbf{k}'_1,+}\big) \\
& \times \big(V_{12}\hat{A}_{1,\mathbf{k}_2,+} + V_{22}\hat{A}_{2,\mathbf{k}_2,+} + V_{32}\hat{A}_{3,\mathbf{k}_2,+}\big)\big(V_{12}\hat{A}_{1,\mathbf{k}_1,+} + V_{22}\hat{A}_{2,\mathbf{k}_1,+} + V_{32}\hat{A}_{3,\mathbf{k}_1,+}\big) + \alpha^{\mathrm{DD}}_1\big(V_{12}\hat{A}^\dagger_{1,\mathbf{k}'_2,-} \\
& + V_{22}\hat{A}^\dagger_{2,\mathbf{k}'_2,-} + V_{32}\hat{A}^\dagger_{3,\mathbf{k}'_2,-}\big)\big(V_{12}\hat{A}^\dagger_{1,\mathbf{k}'_1,-} + V_{22}\hat{A}^\dagger_{2,\mathbf{k}'_1,-} + V_{32}\hat{A}^\dagger_{3,\mathbf{k}'_1,-}\big)\big(V_{12}\hat{A}_{1,\mathbf{k}_2,-} + V_{22}\hat{A}_{2,\mathbf{k}_2,-} + V_{32}\hat{A}_{3,\mathbf{k}_2,-}\big) \\
& \times \big(V_{12}\hat{A}_{1,\mathbf{k}_1,-} + V_{22}\hat{A}_{2,\mathbf{k}_1,-} + V_{32}\hat{A}_{3,\mathbf{k}_1,-}\big) + \alpha^{\mathrm{DD}}_2\big(V_{12}\hat{A}^\dagger_{1,\mathbf{k}'_2,+} + V_{22}\hat{A}^\dagger_{2,\mathbf{k}'_2,+} + V_{32}\hat{A}^\dagger_{3,\mathbf{k}'_2,+}\big) \\
& \times \big(V_{12}\hat{A}_{1,\mathbf{k}_2,+} + V_{22}\hat{A}_{2,\mathbf{k}_2,+} + V_{32}\hat{A}_{3,\mathbf{k}_2,+}\big)\big(V_{12}\hat{A}^\dagger_{1,\mathbf{k}'_1,-} + V_{22}\hat{A}^\dagger_{2,\mathbf{k}'_1,-} + V_{32}\hat{A}^\dagger_{3,\mathbf{k}'_1,-}\big)\big(V_{12}\hat{A}_{1,\mathbf{k}_1,-} + V_{22}\hat{A}_{2,\mathbf{k}_1,-} + V_{32}\hat{A}_{3,\mathbf{k}_1,-}\big) \\
& + \alpha^{\mathrm{DD}}_2\big(V_{12}\hat{A}^\dagger_{1,\mathbf{k}'_2,-} + V_{22}\hat{A}^\dagger_{2,\mathbf{k}'_2,-} + V_{32}\hat{A}^\dagger_{3,\mathbf{k}'_2,-}\big)\big(V_{12}\hat{A}_{1,\mathbf{k}_2,-} + V_{22}\hat{A}_{2,\mathbf{k}_2,-} + V_{32}\hat{A}_{3,\mathbf{k}_2,-}\big) \\
& \times \big(V_{12}\hat{A}^\dagger_{1,\mathbf{k}'_1,+} + V_{22}\hat{A}^\dagger_{2,\mathbf{k}'_1,+} + V_{32}\hat{A}^\dagger_{3,\mathbf{k}'_1,+}\big)\big(V_{12}\hat{A}_{1,\mathbf{k}_1,+} + V_{22}\hat{A}_{2,\mathbf{k}_1,+} + V_{32}\hat{A}_{3,\mathbf{k}_1,+}\big).
\end{aligned} \tag{C12}$$

To proceed, we recall the relevant quantum and classical modes required for the operation of a serial multimode CNOT gate shown for example in Fig. 3. Associating the UP, MP, and LP modes with $\hat{A}_1$, $\hat{A}_2$, and $\hat{A}_3$ modes, the generic interaction Hamiltonian (C12) can be accommodated to our needs using the set of relabelings:

$$\begin{aligned}
&\hat{A}_{1,\mathbf{k}_1,+} \mapsto \psi_{\text{UP},+}, \quad \hat{A}_{1,\mathbf{k}_1,-} \mapsto 0, \quad \hat{A}_{1,\mathbf{k}_2,+} \mapsto 0, \quad \hat{A}_{1,\mathbf{k}_2,-} \mapsto 0, \quad \hat{A}_{2,\mathbf{k}_1,+} \mapsto \hat{a}_{1,+}, \quad \hat{A}_{2,\mathbf{k}_1,-} \mapsto \hat{a}_{1,-}, \\
&\hat{A}_{2,\mathbf{k}_2,+} \mapsto \hat{a}_{2,+}, \quad \hat{A}_{2,\mathbf{k}_2,-} \mapsto \hat{a}_{2,-}, \quad \hat{A}_{3,\mathbf{k}_1,+} \mapsto 0, \quad \hat{A}_{3,\mathbf{k}_1,-} \mapsto \psi'_{\text{LP},-}, \quad \hat{A}_{3,\mathbf{k}_2,+} \mapsto \psi_{\text{LP},+}, \quad \hat{A}_{3,\mathbf{k}_2,-} \mapsto \psi_{\text{LP},-},
\end{aligned} \tag{C13}$$

and again the final-state (primed) wave vectors are chosen according to momentum-conservation rules. These imply that $\mathbf{k}_1 + \mathbf{k}_2 = \mathbf{k}'_2 + \mathbf{k}'_1$ for parametric coupling processes and $\mathbf{k}_2 - \mathbf{k}_1 = \mathbf{k}'_2 - \mathbf{k}'_1$ for linear coupling processes, which can always be satisfied by choosing wave vectors for the classical modes appropriately.

Using Eq. (C13), we can rewrite Eq. (C12) as

$$\begin{aligned}
\hat{\mathcal{H}}'_{\text{DX-DX}} = {} & \alpha^{\mathrm{DD}}_1(V_{22}\hat{a}^\dagger_{2,+} + V_{32}\psi^*_{\text{LP},+})(V_{12}\psi^*_{\text{UP},+} + V_{22}\hat{a}^\dagger_{1,+})(V_{12}\psi_{\text{UP},+} + V_{22}\hat{a}_{1,+})(V_{22}\hat{a}_{2,+} + V_{32}\psi_{\text{LP},+}) \\
& + \alpha^{\mathrm{DD}}_1(V_{22}\hat{a}^\dagger_{2,-} + V_{32}\psi^*_{\text{LP},-})(V_{22}\hat{a}^\dagger_{1,-} + V_{32}\psi'^*_{\text{LP},-})(V_{22}\hat{a}_{1,-} + V_{32}\psi'_{\text{LP},-})(V_{22}\hat{a}_{2,-} + V_{32}\psi_{\text{LP},-}) \\
& + \alpha^{\mathrm{DD}}_2(V_{22}\hat{a}^\dagger_{2,+} + V_{32}\psi^*_{\text{LP},+})(V_{12}\psi_{\text{UP},+} + V_{22}\hat{a}_{1,+})(V_{22}\hat{A}^\dagger_{1,-} + V_{32}\psi'^*_{\text{LP},-})(V_{22}\hat{A}_{2,-} + V_{32}\psi_{\text{LP},-}) \\
& + \alpha^{\mathrm{DD}}_2(V_{22}\hat{a}^\dagger_{2,-} + V_{32}\psi^*_{\text{LP},-})(V_{22}\hat{a}_{1,-} + V_{32}\psi'_{\text{LP},-})(V_{12}\psi^*_{\text{UP},+} + V_{22}\hat{a}^\dagger_{1,+})(V_{22}\hat{a}_{2,+} + V_{32}\psi_{\text{LP},+}).
\end{aligned} \tag{C14}$$

Taking only energy-conserving terms, we arrive at the Hamiltonian derived from the DX-DX interaction:

$$\begin{aligned}\hat{\mathcal{H}}'_{\text{DX-DX}} = {}& \alpha_1^{\text{DD}}\left(V_{22}^2 V_{12} V_{32}\psi_{\text{UP},+}\psi_{\text{LP},+}\hat{a}_{2,+}^\dagger\hat{a}_{1,+}^\dagger + \text{H.c.}\right) + \alpha_1^{\text{DD}}\left(V_{22}^2 V_{32}^2\psi'^*_{\text{LP},-}\psi_{\text{LP},-}\hat{a}_{2,-}^\dagger\hat{a}_{1,-} + \text{H.c.}\right)\\ &+ \alpha_2^{\text{DD}}\left(V_{22}^2 V_{12} V_{32}\psi_{\text{UP},+}\psi_{\text{LP},-}\hat{a}_{2,+}^\dagger\hat{a}_{1,-}^\dagger + \text{H.c.}\right) + \alpha_2^{\text{DD}}\left(V_{22}^2 V_{32}^2\psi^*_{\text{LP},-}\psi'_{\text{LP},-}\hat{a}_{1,+}^\dagger\hat{a}_{2,+} + \text{H.c.}\right)\\ &+ \alpha_2^{\text{DD}}\left(V_{22}^2 V_{32}^2\psi^*_{\text{LP},+}\psi_{\text{LP},-}\hat{a}_{1,-}^\dagger\hat{a}_{1,+} + \text{H.c.}\right).\end{aligned} \tag{C15}$$

A similar procedure can be applied to IX-IX and DX-IX interactions, leading to the transformed interaction Hamiltonian of the form

$$\begin{aligned}\hat{\mathcal{H}}'_{\text{int}} = {}& (A\psi_{\text{UP},+}\psi_{\text{LP},+}\hat{a}_{2,+}^\dagger\hat{a}_{1,+}^\dagger + \text{H.c.}) + (B\psi'^*_{\text{LP},-}\psi_{\text{LP},-}\hat{a}_{2,-}^\dagger\hat{a}_{1,-} + \text{H.c.}) + (C\psi_{\text{UP},+}\psi_{\text{LP},-}\hat{a}_{2,+}^\dagger\hat{a}_{1,-}^\dagger + \text{H.c.})\\ &+ (D\psi'^*_{\text{LP},-}\psi_{\text{LP},-}\hat{a}_{2,+}^\dagger\hat{a}_{1,+} + \text{H.c.}) + (E\psi^*_{\text{LP},+}\psi_{\text{LP},-}\hat{a}_{1,-}^\dagger\hat{a}_{1,+} + \text{H.c.}),\end{aligned} \tag{C16}$$

where we defined the constants

$$\begin{aligned}A &= \alpha_1^{\text{DD}}V_{22}^2V_{12}V_{32} + \alpha_1^{\text{II}}V_{23}^2V_{13}V_{33} + \alpha_1^{\text{DI}}V_{22}V_{23}V_{12}V_{33},\\ B &= \alpha_1^{\text{DD}}V_{22}^2V_{32}^2 + \alpha_1^{\text{II}}V_{23}^2V_{33}^2 + \alpha_1^{\text{DI}}V_{22}^2V_{33}^2,\\ C &= \alpha_2^{\text{DD}}V_{22}^2V_{12}V_{32} + \alpha_2^{\text{II}}V_{23}^2V_{13}V_{33} + \alpha_2^{\text{DI}}V_{22}V_{23}V_{12}V_{32},\\ D &= \alpha_2^{\text{DD}}V_{22}^2V_{32}^2 + \alpha_2^{\text{II}}V_{23}^2V_{33}^2 + \alpha_2^{\text{DI}}V_{23}^2V_{32}^2,\\ E &= \alpha_2^{\text{DD}}V_{22}^2V_{32}^2 + \alpha_2^{\text{II}}V_{23}^2V_{33}^2 + \alpha_2^{\text{DI}}V_{22}V_{23}V_{33}^2.\end{aligned} \tag{C17}$$

To achieve the desired interaction between quantum modes, we perform a polarization transformation from the circular to linear basis, accounting for the TE-TM splitting, which is present in exciton-polaritonic systems. The transformation reads

$$\hat{a}_{n,+} = \frac{1}{\sqrt{2}}(\hat{a}_{n,\text{TM}}e^{2i\phi_n} + i\hat{a}_{n,\text{TE}}e^{2i\phi_j}), \quad \hat{a}_{n,-} = \frac{1}{\sqrt{2}}(\hat{a}_{n,\text{TM}}e^{-2i\phi_n} - i\hat{a}_{n,\text{TE}}e^{-2i\phi_n}), \tag{C18}$$

where ϕ_n ($n = 1,2$) represent angles encoding momentum states. We are mainly interested in the TM interaction terms (target quantum modes $\hat{a}_{1,\text{TM}}$ and $\hat{a}_{2,\text{TM}}$), while TE modes as well as cross-terms can be disregarded in the case of large TE-TM splitting (see the discussion in the next section). Also, we write the classically driven modes ψ_j explicitly as complex numbers with the absolute value of Ψ_j and phase ϕ_j, namely

$$\psi_{\text{UP},+} = \Psi_{\text{UP},+}e^{i\phi_{\text{UP},+}}, \quad \psi_{\text{LP},+} = \Psi_{\text{LP},+}e^{i\phi_{\text{LP},+}}, \quad \psi_{\text{LP},-} = \Psi_{\text{LP},-}e^{i\phi_{\text{LP},-}}, \quad \psi'_{\text{LP},-} = \Psi'_{\text{LP},-}e^{i\phi'_{\text{LP},-}}. \tag{C19}$$

Performing the transformation of Hamiltonian (C16), we obtain

$$\begin{aligned}\hat{\mathcal{H}}''_{\text{int}} = {}& \left[\frac{A}{2}\Psi_{\text{UP},+}\Psi_{\text{LP},+}e^{i(\phi_{\text{UP},+}+\phi_{\text{LP},+}-2\phi_2-2\phi_1)} + \frac{C}{2}\Psi_{\text{UP},+}\Psi_{\text{LP},-}e^{i(\phi_{\text{UP},+}+\phi_{\text{LP},-}-2\phi_2+2\phi_1)}\right]\hat{a}_{2,\text{TM}}^\dagger\hat{a}_{1,\text{TM}}^\dagger\\ &+ \left[\frac{B}{2}\Psi'_{\text{LP},-}\Psi_{\text{LP},-}e^{i(\phi_{\text{LP},-}-\phi'_{\text{LP},-}+2\phi_2-2\phi_1)} + \frac{D}{2}\Psi'_{\text{LP},-}\Psi_{\text{LP},-}e^{i(\phi_{\text{LP},-}-\phi'_{\text{LP},-}-2\phi_2+2\phi_1)}\right]\hat{a}_{2,\text{TM}}^\dagger\hat{a}_{1,\text{TM}}\\ &+ \frac{E}{2}\Psi_{\text{LP},+}\Psi_{\text{LP},-}e^{i(\phi_{\text{LP},-}-\phi_{\text{LP},+}+4\phi_1)}\hat{a}_{1,\text{TM}}^\dagger\hat{a}_{1,\text{TM}} + \text{H.c.},\end{aligned} \tag{C20}$$

where the first two terms correspond to useful parametric and linear coupling terms, and the third term represents an additional energy shift of one of the modes. Finally, to reduce the system to the required $\hat{q}_1\hat{p}_2$ type of interaction, the phases of the classical drives can be adjusted to make each term in Eq. (C20) purely imaginary. This can be satisfied with two sets of conditions defined by the right-hand side of Eq. (C24):

$$e^{i(\phi_{\text{UP},+}+\phi_{\text{LP},+}-2\phi_2-2\phi_1)} = i, \tag{C21}$$

$$e^{i(\phi_{\text{UP},+}+\phi_{\text{LP},-}-2\phi_2+2\phi_1)} = i, \tag{C22}$$

$$e^{i(\phi_{\text{LP},-}-\phi'_{\text{LP},-}+2\phi_2-2\phi_1)} = i, \tag{C23}$$

$$e^{i(\phi_{\text{LP},-}-\phi'_{\text{LP},-}-2\phi_2+2\phi_1)} = \pm i. \tag{C24}$$

The first system of equations (with plus sign) can be satisfied for

$$\phi_2 = \phi_1 + n\pi/2, \quad \phi_{\mathrm{UP},+} = -\phi_{\mathrm{LP},-} + (2n+1)\pi/2, \quad \phi_{\mathrm{LP},+} = \phi_{\mathrm{LP},-} + 4\phi_1, \quad \phi'_{\mathrm{LP},-} = \phi_{\mathrm{LP},-} - (2n+1)\pi/2, \quad \text{(C25)}$$

and we have the freedom in choosing the $\phi_{\mathrm{LP},-}$ phase. For this choice of phases, the interaction constant shall be tuned to $(A\Psi_{\mathrm{UP},+}\Psi_{\mathrm{LP},+} + C\Psi_{\mathrm{UP},+}\Psi_{\mathrm{LP},-})/2 = (B+D)\Psi'_{\mathrm{LP},-}\Psi_{\mathrm{LP},-}/2 \equiv J$.

The second system of equations (with a minus sign) can be satisfied for

$$\phi_2 = \phi_1 + n\pi/2 + \pi/4, \quad \phi_{\mathrm{UP},+} = -\phi_{\mathrm{LP},-} + (n+1)\pi, \quad \phi_{\mathrm{LP},+} = \phi_{\mathrm{LP},-} + 4\phi_1, \quad \phi'_{\mathrm{LP},-} = \phi_{\mathrm{LP},-} - n\pi/2, \quad \text{(C26)}$$

with the interaction constant tuned to $(A\Psi_{\mathrm{UP},+}\Psi_{\mathrm{LP},+} + C\Psi_{\mathrm{UP},+}\Psi_{\mathrm{LP},-})/2 = (B-D)\Psi'_{\mathrm{LP},-}\Psi_{\mathrm{LP},-}/2 \equiv J$. Accounting for the possibility to modify the system on the fly with adjustable pumps, we can in principle organize a sequence of gates between eight different momentum modes $\Phi_1 = \{\phi_1, \phi_1 + \pi/4, \ldots, \phi_1 + 7\pi/4\}$ characterized by wave vectors $\mathbf{k}_1$. Finally, coupling to another subspace of continuous-wave modes Φ'_1 defined by ϕ'_1 can be done with lower fidelity and exploiting error correction afterwards.

Given the versatility of the system, we can efficiently control the couplings by classical drive amplitudes, and thus arrange the $\hat{\mathcal{H}} = 2J\hat{q}_{1,\mathrm{TM}}\hat{p}_{2,\mathrm{TM}}$ Hamiltonian for original interaction constants $\alpha^{nm}_{1,2}$ ($nm = \mathrm{DD,II,DI}$), including both triplet and singlet interactions. Additionally, the phase conditions set the $\hat{a}^\dagger_{1,\mathrm{TM}}\hat{a}_{1,\mathrm{TM}}$ energy shift to $E\Psi_{\mathrm{LP},+}\Psi_{\mathrm{LP},-}$, implying that it will be minimized by weak drive conditions for $\psi_{\mathrm{LP},+}$ and $\psi_{\mathrm{LP},-}$ classical modes and stronger pumping of $\psi_{\mathrm{UP},+}$ and $\psi'_{\mathrm{LP},-}$ modes.

APPENDIX D: MULTIGATE REALIZATION: TE-MODE INFLUENCE

Now, let us return to the question of the validity of the rotating-wave approximation (RWA) for the TE-TM cross-interaction terms. So far we kept only TM modes, assuming that the TE-TM interaction is strongly suppressed due to the energy shift of TE modes, i.e., TE-TM splitting. However, if the splitting $\Delta_{\text{TE-TM}}$ is small compared to other relevant energy scales (interaction constants and decay rate), this assumption becomes invalid. To test the limits in which auxiliary TE modes can be neglected, we recall that together with useful terms appearing in Eq. (C20), various spurious terms appear, namely $\epsilon_{11}\hat{a}^\dagger_{1,\mathrm{TE}}\hat{a}_{1,\mathrm{TE}}$, $\epsilon_{22}\hat{a}^\dagger_{2,\mathrm{TE}}\hat{a}_{2,\mathrm{TE}}$, $(\epsilon_{12}\hat{a}^\dagger_{1,\mathrm{TE}}\hat{a}_{2,\mathrm{TE}}+\mathrm{H.c.})$, $(\eta_{21}\hat{a}^\dagger_{1,\mathrm{TM}}\hat{a}^\dagger_{2,\mathrm{TE}}+\mathrm{H.c})$, $(\eta_{12}\hat{a}^\dagger_{1,\mathrm{TM}}\hat{a}^\dagger_{1,\mathrm{TE}}+\mathrm{H.c})$, $(\zeta_{21}\hat{a}^\dagger_{2,\mathrm{TM}}\hat{a}_{1,\mathrm{TE}}+\mathrm{H.c})$, etc. Here constants ϵ_{ij}, η_{ij}, and ζ_{ij} denote generic coupling represented by functions of bare interactions, Hopfield coefficients, and classical drive amplitudes. The first three terms act fully in the extra subspace of TE modes and are irrelevant for our considerations. However, the terms of fourth type, fifth type, and so on produce the parasitic rotation for the system modes $\hat{a}_{1/2,\mathrm{TM}}$, or alternatively effective leakage to the TE mode subspace. The related fidelity degradation of the gate then depends on the values of couplings, mode detuning $\Delta_{\text{TE-TM}}$, and decay of the mode.

To quantify the fidelity change due to additional couplings, we refrain from considering a particular system with defined coupling, but we characterize the generic influence of, e.g., η-type coupling. For this, we consider the Hamiltonian

$$\begin{aligned}\hat{\mathcal{H}} = J(&-i\hat{a}_{1,\mathrm{TM}}\hat{a}_{2,\mathrm{TM}} + i\hat{a}^\dagger_{1,\mathrm{TM}}\hat{a}^\dagger_{2,\mathrm{TM}} - i\hat{a}^\dagger_{1,\mathrm{TM}}\hat{a}_{2,\mathrm{TM}} \\ &+ i\hat{a}^\dagger_{2,\mathrm{TM}}\hat{a}_{1,\mathrm{TM}}) + \eta(\hat{a}^\dagger_{2,\mathrm{TM}}\hat{a}^\dagger_{1,\mathrm{TE}} + \mathrm{H.c.}) \\ &+ \Delta\hat{a}^\dagger_{1,\mathrm{TE}}\hat{a}_{1,\mathrm{TE}}, \end{aligned} \quad \text{(D1)}$$

where Δ is a generic TE mode shift defined by TE-TM splitting and nonlinear contribution. Here, for the sake of simplicity, let us rename modes as $\hat{a}_{1,\mathrm{TM}} \equiv \hat{a}_1$, $\hat{a}_{2,\mathrm{TM}} \equiv \hat{a}_2$, and $\hat{a}_{1,\mathrm{TE}} \equiv \hat{a}_3$. Next, Eq. (D1) can be rewritten using position and momentum operators $\hat{q}_j$ and $\hat{p}_j$ associated with each mode, which gives

$$\hat{\mathcal{H}} = 2J\hat{q}_1\hat{p}_2 - \eta(\hat{q}_2\hat{p}_3 + \hat{p}_2\hat{q}_3) + \frac{\Delta}{2}(\hat{q}_3^2 + \hat{p}_3^2). \quad \text{(D2)}$$

Deriving the equations of motion for average amplitudes $\langle\hat{q}_j\rangle, \langle\hat{p}_j\rangle$ ($j = 1,2,3$) and associated correlators, we can calculate the fidelity for the CNOT gate acting in the $\{\hat{a}_1, \hat{a}_2\}$ mode subspace as a function of dimensionless parameters η/J and Δ/J.

The results are shown in Fig. 5, where we considered the cavity decay rate to be small, $\Gamma/J \ll 1$. We see that even for spurious interaction constants η being comparable to coupling J, the degradation of fidelity can be suppressed by the shift of the TE mode. In particular, taking $J = 0.1$ meV for a dipolaritonic system, and assuming realistic 0.5 meV TE-TM splitting, one can achieve the 0.99 fidelity commensurable with previously anticipated degradation due to decay of the cavity mode.

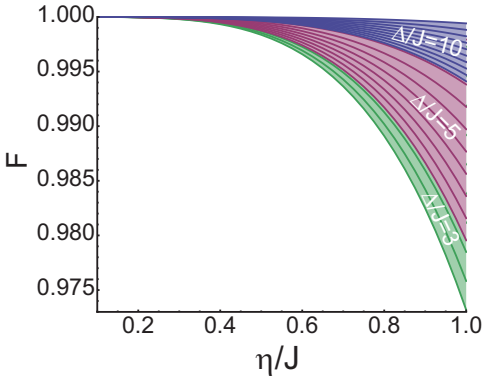

FIG. 5. Influence of a spurious TE-TM coupling on the fidelity of a multimode CNOT gate. The minimal fidelity is shown as a function of additional coupling η for various mode occupations ($\langle x\rangle^2 = 1$ to 10), and three values of dimensionless TE-TM splitting.

[1] L. M. K. Vandersypen, M. Steffen, G. Breyta, C. S. Yannoni, M. H. Sherwood, and I. L. Chuang, Experimental realization of Shor's quantum factoring algorithm using nuclear magnetic resonance, Nature (London) **414**, 883 (2001).

[2] J. L. O'Brien, G. J. Pryde, A. G. White, T. C. Ralph, and D. Branning, Demonstration of an all-optical quantum controlled-NOT gate, Nature (London) **426**, 264 (2003).

[3] A. Politi, J. C. F. Matthews, and J. L. O'Brien, Shors quantum factoring algorithm on a photonic chip, Science **325**, 1221 (2009).

[4] J. Benhelm, G. Kirchmair, C. F. Roos, and R. Blatt, Towards fault-tolerant quantum computing with trapped ions, Nat. Phys. **4**, 463 (2008).

[5] R. Blatt and D. Wineland, Entangled states of trapped atomic ions, Nature (London) **453**, 1008 (2008).

[6] C. Monroe and J. Kim, Scaling the ion trap quantum processor, Science **339**, 1164 (2013).

[7] T. P. Harty, D. T. C. Allcock, C. J. Ballance, L. Guidoni, H. A. Janacek, N. M. Linke, D. N. Stacey, and D. M. Lucas, High-Fidelity Preparation, Gates, Memory, and Readout of a Trapped-Ion Quantum Bit, Phys. Rev. Lett. **113**, 220501 (2014).

[8] T. van der Sar, Z. H. Wang, M. S. Blok, H. Bernien, T. H. Taminiau, D. M. Toyli, D. A. Lidar, D. D. Awschalom, R. Hanson, and V. V. Dobrovitski, Decoherence-protected quantum gates for a hybrid solid-state spin register, Nature (London) **484**, 82 (2012).

[9] L. Di Carlo, J. M. Chow, J. M. Gambetta, L. S. Bishop, B. R. Johnson, D. I. Schuster, J. Majer, A. Blais, L. Frunzio, S. M. Girvin, and R. J. Schoelkopf, Demonstration of two-qubit algorithms with a superconducting quantum processor, Nature (London) **460**, 240 (2009).

[10] A. Federov, L. Steffen, M. Baur, M. P. da Silva, and A. Wallraff, Implementation of a Toffoli gate with superconducting circuits, Nature (London) **481**, 170 (2012).

[11] L. Steffen, Y. Salathe, M. Oppliger, P. Kurpiers, M. Baur, C. Lang, C. Eichler, G. Puebla-Hellmann, A. Federov, and A. Wallraff, Deterministic quantum teleportation with feed-forward in a solid state system, Nature (London) **500**, 319 (2013).

[12] R. Barends *et al.*, Superconducting quantum circuits at the surface code threshold for fault tolerance, Nature (London) **508**, 500 (2014).

[13] J.-Ph. Karr, A. Baas, R. Houdré, and E. Giacobino, Squeezing in semiconductor microcavities in the strong-coupling regime, Phys. Rev. A **69**, 031802(R) (2004).

[14] S. Savasta, R. Girlanda, and G. Martino, Hyper Raman scattering in microcavity quantum wells: A quantum optical process in the strong coupling regime, Phys. Status Solidi A **164**, 85 (1997).

[15] P. Schwendimann, C. Ciuti, and A. Quattropani, Statistics of polaritons in the nonlinear regime, Phys. Rev. B **68**, 165324 (2003).

[16] A. Verger, I. Carusotto, and C. Ciuti, Quantum Monte Carlo study of ring-shaped polariton parametric luminescence in a semiconductor microcavity, Phys. Rev. B **76**, 115324 (2007).

[17] S. Savasta, O. Di Stefano, V. Savona, and W. Langbein, Quantum Complementarity of Microcavity Polaritons, Phys. Rev. Lett. **94**, 246401 (2005).

[18] S. S. Demirchyan, I. Yu. Chestnov, A. P. Alodjants, M. M. Glazov, and A. V. Kavokin, Qubits Based on Polariton Rabi Oscillators, Phys. Rev. Lett. **112**, 196403 (2014).

[19] D. D. Solnyshkov, O. Bleu, and G. Malpuech, All optical controlled-NOT quantum gate based on an exciton-polariton circuit, Superlatt. Microstruct. **83**, 466 (2015).

[20] A. Verger, C. Ciuti, and I. Carusotto, Polariton quantum blockade in a photonic dot, Phys. Rev. B **73**, 193306 (2006).

[21] T. C. H. Liew and V. Savona, Single Photons from Coupled Quantum Modes, Phys. Rev. Lett. **104**, 183601 (2010).

[22] M. Bamba, A. Imamoglu, I. Carusotto, and C. Ciuti, Origin of strong photon antibunching in weakly nonlinear photonic molecules, Phys. Rev. A **83**, 021802(R) (2011).

[23] M. Bamba and C. Ciuti, Counter-polarized single-photon generation from the auxiliary cavity of a weakly nonlinear photonic molecule, Appl. Phys. Lett. **99**, 171111 (2011).

[24] H. Flayac, and V. Savona, Input-output theory of the unconventional photon blockade, Phys. Rev. A **88**, 033836 (2013).

[25] T. C. H. Liew and V. Savona, Multimode entanglement in coupled cavity arrays, New J. Phys. **15**, 025015 (2013).

[26] H. J. Kimble, The quantum internet, Nature (London) **453**, 1023 (2008).

[27] A. Amo, J. Lefrère, S. Pigeon, C. Adrados, C. Ciuti, I. Carusotto, R. Houdré, E. Giacobino, and A. Bramati, Superfluidity of polaritons in semiconductor microcavities, Nat. Phys. **5**, 805 (2009).

[28] A. Amo, D. Sanvitto, F. P. Laussy, D. Ballarini, E. del Valle, M. D. Martin, A. Lemaître, J. Bloch, D. N. Krizhanovskii, M. S. Skolnick, C. Tejeder, and L. Viña, Collective fluid dynamics of a polariton condensate in a semiconductor microcavity, Nature (London) **457**, 291 (2009).

[29] D. Sanvitto, F. M. Marchetti, M. H. Szymańska, G. Tosi, M. Baudisch, F. P. Laussy, D. N. Krizhanovskii, M. S. Skolnick, L. Marrucci, A. Lemaître, J. Bloch, C. Tejedor, and L. Viña, Persistent currents and quantized vortices in a polariton superfluid, Nat. Phys. **6**, 527 (2010).

[30] M. Sich, D. N. Krizhanovskii, M. S. Skolnick, A. V. Gorbach, R. Hartley, D. V. Skryabin, E. A. Cerda-Méndez, K. Biermann, R. Hey, and P. V. Santos, Observation of bright polariton solitons in a semiconductor microcavity, Nat. Photon. **6**, 50 (2012).

[31] O. A. Egorov, A. V. Gorbach, F. Lederer, and D. V. Skryabin, Two-Dimensional Localization of Exciton Polaritons in Microcavities, Phys. Rev. Lett. **105**, 073903 (2010).

[32] T. Espinosa-Ortega and T. C. H. Liew, Perceptrons with Hebbian Learning Based on Wave Ensembles in Spatially Patterned Potentials, Phys. Rev. Lett. **114**, 118101 (2015).

[33] S. L. Braunstein and P. van Loock, Quantum information with continuous variables, Rev. Mod. Phys. **77**, 513 (2005).

[34] S. L. Braunstein, Error Correction for Continuous Quantum Variables, Phys. Rev. Lett. **80**, 4084 (1998).

[35] C. Ciuti, Branch-entangled polariton pairs in planar microcavities and photonic wires, Phys. Rev. B **69**, 245304 (2004).

[36] C.-E. Bardyn and A. İmamoğlu, Majorana-Like Modes of Light in a One-Dimensional Array of Nonlinear Cavities, Phys. Rev. Lett. **109**, 253606 (2012).

[37] C. Diederichs, J. Tignon, G. Dasbach, C. Ciuti, A. Lemaître, J. Bloch, Ph. Roussignol, and C. Delalande, Parametric oscillation in vertical triple microcavities, Nature (London) **440**, 904 (2006).

[38] A. Amo, S. Pigeon, C. Adrados, R. Houdré, E. Giacobino, C. Ciuti, and A. Bramati, Light engineering of the polariton landscape in semiconductor microcavities, Phys. Rev. B **82**, 081301(R) (2010).

[39] E. Wertz, L. Ferrier, D. Solnyshkov, R. Johne, D. Sanvitto, A. Lemaître, I. Sagnes, R. Grousson, A. V. Kavokin, P. Senellart, G. Malpuech, and J. Bloch, Spontaneous formation and optical manipulation of extended polariton condensates, Nat. Phys. **6**, 860 (2010).

[40] G. Tosi, G. Christmann, N. G. Berloff, P. Tsotsis, T. Gao, Z. Hatzopoulos, P. G. Savvidis, and J. J. Baumberg, Sculpting oscillators with light within a nonlinear quantum fluid, Nat. Phys. **8**, 190 (2012).

[41] T. Gao, P. S. Eldridge, T. C. H. Liew, S. I. Tsintzos, G. Stavrinidis, G. Deligeorgis, Z. Hatzopoulos, and P. G. Savvidis, Polariton condensate transistor switch, Phys. Rev. B **85**, 235102 (2012).

[42] J. Schmutzler, P. Lewandowski, M. Assmann, D. Niemietz, S. Schumacher, M. Kamp, C. Schneider, S. Höfling, and M. Bayer, All-optical flow control of a polariton condensate using nonresonant excitation, Phys. Rev. B **91**, 195308 (2015).

[43] O. Kyriienko and T. C. H. Liew, Triggered single-photon emitters based on stimulated parametric scattering in weakly nonlinear systems, Phys. Rev. A **90**, 063805 (2014).

[44] J. Keeling and N. G. Berloff, Spontaneous Rotating Vortex Lattices in a Pumped Decaying Condensate, Phys. Rev. Lett. **100**, 250401 (2008).

[45] P. Marian and T. A. Marian, Uhlmann fidelity between two-mode Gaussian states, Phys. Rev. A **86**, 022340 (2012).

[46] G. Spedalieri, C. Weedbrook, and S. Pirandola, A limit formula for the quantum fidelity, J. Phys. A **46**, 025304 (2013).

[47] B. Nelson, G. Liu, M. Steger, D. W. Snoke, R. Balili, K. West, and L. Pfeiffer, Dissipationless flow and sharp threshold of a polariton condensate with long lifetime, Phys. Rev. X **3**, 041015 (2013).

[48] M. Steger, C. Gautham, D. W. Snoke, L. Pfeiffer, and K. West, Slow reflection and two-photon generation of microcavity exciton polaritons, Optica **2**, 1 (2015).

[49] V. Savona and C. Piermarocchi, Microcavity polaritons: Homogeneous and inhomogeneous broadening in the strong coupling regime, Phys. Status Solidi A **164**, 45 (1997).

[50] P. Crisofolini, G. Christmann, S. I. Tsintzos, G. Deligeorgis, G. Konstantinidis, Z. Hatzopoulos, P. G. Savvidis, and J. J. Baumberg, Coupling quantum tunneling with cavity photons, Science **336**, 704 (2012).

[51] G. Panzarini, L. C. Andreani, A. Armitage, D. Baxter, M. S. Skolnick, V. N. Astratov, J. S. Roberts, A. V. Kavokin, M. R. Vladimirova, and M. A. Kaliteevski, Exciton-light coupling in single and coupled semiconductor microcavities: Polariton dispersion and polarization splitting, Phys. Rev. B **59**, 5082 (1999).

[52] M. Lobino, D. Korystov, C. Kupchak, E. Figueroa, B. C. Sanders, and A. I. Lvovsky, Complete Characterization of Quantum-Optical Processes, Science **322**, 563 (2008).

[53] V. D'Auria, S. Fornaro, A. Porzio, S. Solimeno, S. Olivares, and M. G. A. Paris, Full Characterization of Gaussian Bipartite Entangled States by a Single Homodyne Detector, Phys. Rev. Lett. **102**, 020502 (2009).

[54] T. Byrnes, G. V. Kolmakov, R. Ya. Kezerashvili, and Y. Yamamoto, Effective interaction and condensation of dipolaritons in coupled quantum wells, Phys. Rev. B **90**, 125314 (2014).